

Run and Tumble Dynamics of Biased Quantum Trajectories in a Monitored Qubit

Aritra Kundu 

Department of Physics and Materials Science, University of Luxembourg, L-1511 Luxembourg*

(Dated: December 24, 2025)

We investigate the active stochastic dynamics of a qubit subjected to continuous measurement and conditional feedback. The stochastic equation governing the state vector trajectory of the qubit can be mapped, in the high-diffusion limit, to the dynamics of a classical persistent Run-and-Tumble Particle (p-RTP) in a bounded one-dimensional domain. The mapping enables us to use analytical results from classical active matter to derive an approximate non-equilibrium steady-state (NESS) distribution for the monitored quantum system. The competition between the coherent Rabi drive and the measurement-induced feedback leads to a rich NESS phase displaying Zeno–anti-Zeno transition—which is statistically equivalent to the propulsion-induced trapping observed in confined active particles.

A paradigmatic model in classical active matter is the Run-and-Tumble Particle (RTP) in one dimension, where a particle undergoes persistent motion with a velocity that switches stochastically between discrete states [1, 2]. RTP captures non-equilibrium phenomena emerging from the breaking of the microscopic detail balance. This results in rich collective phenomena, such as propulsion-induced phase separation and ratchet effects, in biological systems that occur on macro-mesoscopic timescales [3–6].

Concurrently, continuous measurement allows tracking of a single quantum trajectory undergoing quantum jumps driven by microscopic quantum evolution. These trajectories evolve stochastically due to the back-action of the measurement feedback [7, 8]. Recent technological advancements enable the observation of non-Hermitian evolution [9] and incomplete quantum jumps, called “spikes” [8]. The statistics of first passage times [10–14] and spikes in diffusive [15–19] or Poissonian trajectories [20] suggests a hidden active character in monitored quantum evolution.

This Letter explores the idea of run-and-tumble motion in quantum trajectories [21] of a two-level quantum system (qubit) under simultaneous coherent driving and continuous detection with feedback. We show that the qubit quantum trajectories on the Bloch sphere coarse-grains to a Fokker–Planck equation identical to that of a persistent run-and-tumble particle in a bounded domain. The approximation becomes more accurate as the noise becomes large. This mathematical equivalence links two disparate systems in physical time: second-scale active motion and sub-microsecond open quantum evolution. This mapping is significant for two reasons. First, it allows us to import statistical results from the active matter literature to shed insights into the statistics of the quantum trajectory. Second, it provides a physical interpretation of the Quantum Zeno effect in terms of active transport: the freezing of the quantum state corresponds to the trapping of an active particle when its propulsion velocity exceeds its active speed. The discrete space quantum system we consider exhibits structural similarity to the non-CPTP map presented in [22], which

studied quantum active matter in continuous-variable systems.

To validate this disparate connection, we analyze the different phases of the steady state distribution for (i) the p-RTP model in a bounded domain $x \in [-\ell, \ell]$ and (ii) a specific setup of the averaged Liouvillian superoperator of a continuously monitored two-level qubit with feedback/bias. The characteristic equation governing the steady-state distribution $P(x)$ and the averaged Liouvillian superoperator of the feedback-controlled density matrix (ρ) takes the form of a cubic equation in Weistereiss form:

$$t^3 + pt + q = 0, \quad (1)$$

Where the discriminant $\Delta_t = -4p^3 - 27q^2 < 0$ ensures real roots, a necessary condition for a physical probability density in the presence of reflective boundaries. In what follows, we first discuss the explicit results of the p-RTP and its steady-state solutions. Later, we discuss our qubit model and its connection to the run-and-tumble dynamics.

Classical Model: Persistent RTP in a Bounded Domain— We consider a particle moving in one dimension $x \in [-\ell, \ell]$ with persistent motion described with the Langevin equation:

$$dx = [v_d + vs(t)]dt + \sqrt{2D}dW_t, \quad (2)$$

where v_d is a constant propulsion velocity, v is the active speed, and $s(t) \in -1, 1$ is a noise flipping at Poisson rate λ . Here, dW_t is a zero mean Wiener process satisfying Ito-rule $dW_t^2 = dt$. The corresponding stationary Fokker–Planck equation with zero-flux reflective boundary conditions [2] give the stationary distribution $P(x)$. Fig. (1)(a) shows a typical trajectory of p-RTP where the instantaneous internal state and also the noise combined determines the local direction of the particle.

Characteristic Equation and Explicit Solution of Steady-state: The steady-state probability density $P(x)$ is a superposition of exponential modes, $e^{(t+\frac{2v_d}{3D})x}$ where t satisfies Eq.(1) where the coefficients p and q are both functions of v, v_d, D, λ [23] [2].

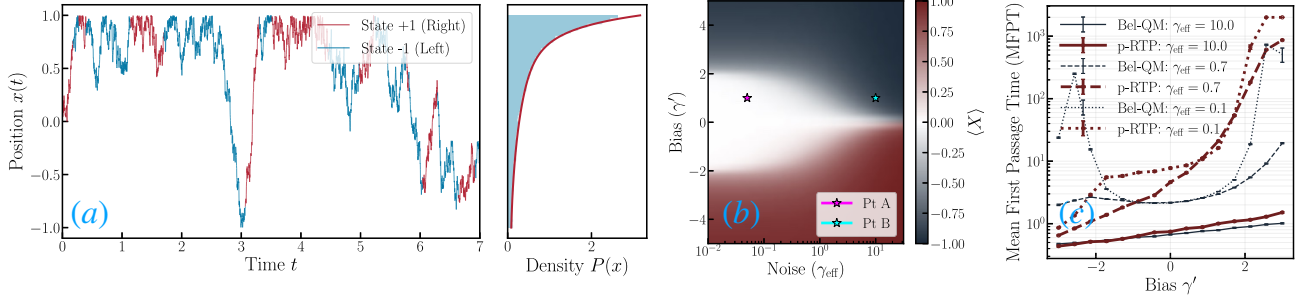


FIG. 1. **Classical-Quantum connection** (a) Single trajectory of the effective coordinate $x(t)$ of p-RTP model from Eq.(2). The red-blue markings reflect the current internal state. (b) Phase diagram showing the transition from Zeno to bimodal Anti-Zeno stationary distributions obtained from stochastic averaged- Eq. (4) (Avg-QM). The effect of the feedback bias γ' acts as a symmetry-breaking drift field. (c) The Mean First Passage Time (MFPT) to the boundary. The maroon lines represent the prediction from the p-RTP model, while black lines represent numerical simulations of the quantum Belavkin SME: Eq.(4) (Bel-QM). The agreement in the high-noise limit validates the effective p-RTP description.

This exact solution matches perfectly with the numerical simulation of the Langevin equation in Fig.1(a) (red line). The piling up of the probability density at the boundaries is reminiscent of non-hermitian skin effects [24].

Asymptotic results: Here, we present explicit results for the low-diffusion ($D \rightarrow 0$) and high-diffusion ($D \rightarrow \infty$) limits. In the low diffusion limit, the density $P(x)$ describes an asymptotic theory combining a smooth exponential bulk,

$$P(x) \propto e^{r_1 x} + m_\delta^\pm \delta(x \pm \ell), \quad (3)$$

with a decay rate $r_1 = \frac{2\lambda v_d}{v^2 - v_d^2}$, and finite, $\mathcal{O}(1)$ delta-function masses m_δ^\pm at the boundary given by the explicit formula:

$$m_\delta^\pm = \frac{1}{2} \frac{v_d}{v} \frac{e^{\pm r_1 \ell}}{\sinh(r_1 \ell) + \frac{v_d}{v} \cosh(r_1 \ell)}.$$

This result generalises of the sedimentation of active-particles to a bounded domain [3, 25]. The characteristic and the length scale diverge when $v_d = v$. In the limit of $D \rightarrow \infty$, the flip becomes irrelevant, and the steady state density reads [27] ,

$$P(x) \approx \frac{1}{2\ell} \left(1 + \frac{v_d}{D} x \right).$$

Next, we turn to the quantum setup of a two-level system continuously monitored and its mapping to the p-RTP model.

Quantum Model: The Monitored Qubit with Feedback—We consider a two-level system, a qubit, described by the Hamiltonian $\hat{H}_0 = J\sigma_x$ and continuously monitored via the projection operator $\hat{L} = \sigma^+\sigma^-$. The monitoring creates back-action due to the non-commutativity of $[\hat{L}, \hat{H}_0] \neq 0$, making it not a quantum nondemolition measurement. Related to this model, [28] studied

the diffusive trajectories, [20] studied the Poissonian trajectories and [29–31] studied zeno dynamics. The setup was realized in the laboratory [9, 32], but no-jump post-selection limits the experiments [26]. The tilted Belavkin-Barchielli-Zakai equation (Bel-QM) [33–37] describes the best estimate of the system’s state through the system’s stochastic density matrix, $\hat{\varrho}$, conditioned on the biased stream of measurement data collected up to time t [27] :

$$d\hat{\varrho} = \mathcal{L}^{\gamma_{\text{eff}}}[\hat{\varrho}]dt + \mathcal{I}^{\gamma_{\text{eff}}, \gamma'}[\hat{\varrho}], \quad (4)$$

where the first term is the average evolution with the standard Lindblad Liouvillian given by:

$$\mathcal{L}^{\gamma_{\text{eff}}}[\hat{\varrho}] = -i[\hat{H}_0, \hat{\varrho}]dt + \gamma_{\text{eff}} \left(2\hat{L}\hat{\varrho}\hat{L}^\dagger - \{\hat{L}^\dagger\hat{L}, \hat{\varrho}\} \right) dt, \quad (5)$$

and the second is the innovation term representing the measurement back-action element given as:

$$\mathcal{I}^{\gamma_{\text{eff}}, \gamma'}[\hat{\varrho}] = \left(\gamma' dt - \sqrt{2\gamma_{\text{eff}}} dW_t \right) \left(\{\hat{L}, \hat{\varrho}\} - \hat{\varrho} \text{Tr}[(\hat{L} + \hat{L}^\dagger)\hat{\varrho}] \right). \quad (6)$$

The “information” collected by the observer (γ') mathematically denotes deviation from the martingale assumptions of the noise. At the same time, γ_{eff} is the effective diffusion constant arising from the measurement back-action. The single-trajectory normalization is routinely studied in [17, 30, 31, 38] for the study of quantum trajectories[39].

For $\gamma' = 0$, the innovation term exactly counterbalances the decoherence from the Lindblad dissipation, preserving the purity of the state. However, when $\gamma' \neq 0$, the innovation bias the fluctuations to create a “propulsion” effect.

The zero-noise limit, when $dW_t \rightarrow 0$, the Liouvillian superoperator (Avg-QM) with the diagonal weights $d_1 = 0$, $d_2 = d_3 = -\gamma_{\text{eff}}/2$, $d_4 = -\gamma'$, the operator

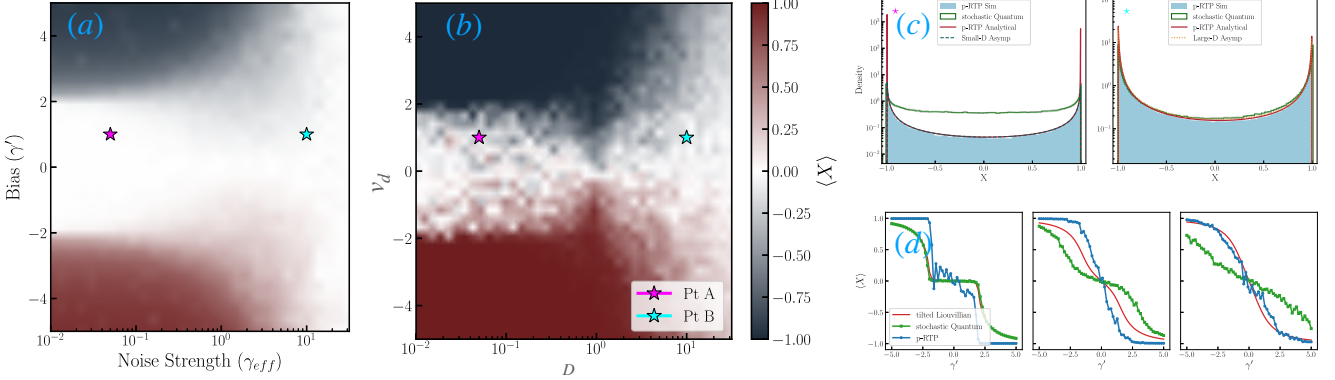


FIG. 2. **Analysis of the steady-state statistics for biased continuous quantum monitoring of a qubit.** (a) Phase diagrams displaying the mean position $\langle X \rangle$ as a function of the effective diffusion rate γ_{eff} and bias parameter γ' . computed from Bel-QM (b). Shows the averaged mean position from the effective p-RTP SDE approximation. The stars mark two specific parameter regimes: Point A (magenta, low diffusion $\gamma_{\text{eff}} = D = 0.05$) and Point B (cyan, high diffusion $\gamma_{\text{eff}} = D = 10.0$). (c) Steady-state probability density distributions $P(X)$ for the parameters corresponding to points A and B for the p-RTP model and the quantum simulation (Bel-QM). The plots compare the p-RTP simulation (blue histogram), the quantum simulation (green line), the exact solution (red line), and the small-diffusion asymptotic approximation (dashed teal line) as formulas given in . The statistics of the phase becomes accurate in the higher diffusion limit where the quantum effects has been washed out as also evidence from the first passage times Fig. 1(c) (d) One-dimensional slices of the phase diagram at fixed diffusion levels ($\gamma_{\text{eff}} = 0.02, 0.7, 2.0$). The curves compare the mean position $\langle X \rangle$ obtained from the tilted Liouvillian evolution (Avg-QM) (purple), the stochastic quantum simulation (Bel-QM) (green), and the hyperbolic transformed p-RTP model Eq.(8) with $\ell = \pi$ (blue).

$(\mathcal{L}^\gamma)[\rho]$ [40] is written compactly as

$$\mathcal{L}^{\gamma_{\text{eff}}} = \sum_{j=1}^4 d_j E_{jj} + \left[i(E_{12} + E_{34} - E_{13} - E_{24}) + \text{h.c.} \right], \quad (7)$$

where $E_{jk} \equiv |j\rangle\langle k|$, $\langle k|j\rangle = \delta_{kj}$ and

the characteristic polynomial takes the form given in Eq.(1) [41]. This already precipitates the previously anticipated structure of the underlying p-RTP model. To uncover the underlying connection, we note that, for the chosen driving and jump operators, the quantum trajectories are restricted to a plane in the Bloch sphere characterized by θ, ϕ . Hence, it is enough to restrict to the Bloch coordinate θ variable. The phase space structure is revealed from the order parameter $X_t = \cos(\theta_t)$. The effective stochastic quantum trajectory follows a dynamics in a washerboard potential reminiscent of motion in superconducting qubits [42, 43].

Information Geometric mapping to Propulsion– The Fubini–Study metric for a pure qubit state on the Bloch sphere is $ds^2 = d\theta^2 + \sin^2 \theta d\phi^2$ [44]. Using Gudermanian transformation $gd(\zeta) = 2 \arctan(e^\zeta) - \pi/2$, satisfying $\sin(gd(\zeta)) = \tanh \zeta$. Defining $\theta = \pi/2 - gd(\zeta)$ yields $\cos \theta = \tanh \zeta$. The metric becomes conformally flat in the ζ coordinates as, $ds^2 = \text{sech}^2 \zeta (d\zeta^2 + d\phi^2)$. The mapping sends the bounded domain $\theta \in (0, \pi)$ to $\zeta \in (-\infty, \infty)$. For numerical stability and to maintain correspondence with the bounded RTP model, we simulate the dynamics of the transformed variable truncated to a domain $x_t \in [-\ell, \ell]$.

The approximate stochastic differential equation (SDE) governs the effective dynamics of the transformed coordinate x_t of the qubit is

$$dx_t \approx [-\gamma' + 2J s(t)] dt + \sqrt{2\gamma_{\text{eff}}} dW_t, \quad (8)$$

where γ' represents the feedback bias. In the high-diffusion limit, the coherent Rabi oscillation is approximated by instantaneous switching events $s(t)$ with an adaptive rate $\lambda(\gamma_{\text{eff}}, J) \approx \frac{J(4/\pi-1)}{\log(\gamma_{\text{eff}})}$. This approximation reflects the physical limit in which the non-Markovian state-dependent flip rate due to coherent oscillation is approximated as a constant, rendering the Rabi drive statistically equivalent to a telegraphic flipping process. The validity of the assumption increases in the large-noise limit. The First-Passage Time statistics shown in Fig. 1 confirms the active picture of the quantum trajectories dynamically. In the high-diffusion limit, the active picture becomes exact, and the quantum solution converges to the p-RTP prediction. We compute the steady-state expectation value $\langle X_t \rangle_{ss} = \langle \tanh(x_t) \rangle_{ss}$ by averaging the back-transformed variable over long-time simulations of Eq. (8).

NESS Zeno-Anti-Zeno phase diagram– We now analyze the non-equilibrium steady-state properties of the system. The feedback-controlled qubit monitoring realizes a Zeno–anti–Zeno crossover initially identified by Misra and Sudarshan [45, 46]. The phase behavior in Figure 2(a), displays the steady-state mean position $\langle X \rangle$ as a function of the effective dissipation rate γ_{eff} and the

bias parameter γ' for the quantum simulation. We see that the classical p-RTP model in Figure 2(b) qualitatively displays captures essential features of the quantum simulation at the average level.

In the regime of significant positive bias $\gamma' \gg J$, the demon strongly favors the subspace aligned with the bias. The dynamics enter a *Zeno-like freezing* regime where transitions are suppressed, and the system becomes localized near the boundary $\langle X \rangle \approx +1$. Symmetrically, a significant negative bias stabilizes the opposite sector $\langle X \rangle \approx -1$. This localization is consistent with the *measurement-modified state selection* predicted in [47, 48].

Between these localized domains, we observe a broad *anti-Zeno regime*. Here, the stochastic back-action from the feedback effectively competes with the deterministic bias, having an effective “activity”. Neither γ' nor γ_{eff} is sufficient to arrest the dynamics; instead, the fluctuations enhance the switching rate, driving the system toward a delocalized steady state with $\langle X \rangle \approx 0$. The crossover to the localized phase occurs approximately when the bias exceeds the coherent drive scale, $|\gamma'| \simeq 2J$, in the limit of weak dissipation $\gamma_{\text{eff}} \lesssim 1$. Fig. (2) shows the full probability distribution of the quantum distribution from Eq.(4) compared to the exact distribution from the p-RTP model Eq. (8) for the two points marked in Fig. (2)(a). The distribution becomes exact as the diffusion constant increases (the measurement becomes weaker).

The competition between deterministic dissipation and stochastic biasing thus defines the phase boundary. As γ' increases, the enhanced fluctuations counteract the dissipative freezing, shifting the transition to larger values of γ_{eff} . Consequently, more substantial dissipation is required to maintain the Zeno subspace in the presence of strong feedback. A closer analysis in Fig. (2)(c,d) reveals that in the small diffusion limit, the quantum-to-classical map identifies the phase transitions at bias strength $\gamma' = \pm 2J$ while the full distribution displays differences due to the quantum-classical transition approximations. In the high-diffusion limit, the classical p-RTP solution for X_t on average matches the solution of the averaged Lindblad equation, and the full distribution matches the latter.

Conclusion— We investigate the active dynamics of biased continuous quantum measurements using stochastic processes with telegraphic noise, and establish an approximate mapping between a continuously monitored qubit under feedback and a persistent run-and-tumble particle confined to a bounded domain. This correspondence provides a mechanism for measurement-induced transport: the Quantum Zeno transition of the qubit is directly analogous to the motility-induced shape transition observed in classical active matter.

Our results show that tools from nonequilibrium statistical mechanics, in particular large-deviation theory and current-fluctuation analysis for RTPs, provide a natural

framework for characterizing the statistics of quantum trajectories. This framework offers a physical interpretation of the Quantum Zeno effect as motility-induced trapping, in which measurement suppresses coherent motion, as confinement does for an active particle. Although we studied this for a specific setup, extending the information geometric picture to more complex setups will be illuminating specially in the case of commuting system and environment operator. Extending this approach to study full-time dynamics and to include non-Markovian flipping rates to capture full dynamics is left for future work.

I thank Raphael Cheterite, Cedric Bernardin, Abhishek Dhar, Pablo Martinez Azcona, and Komal Kumari for valuable discussions on related topics. This work is supported by FNR CORE junior grant no. 17132054. This research was supported in part by the International Centre for Theoretical Sciences (ICTS) for the program Quantum Trajectories (code: ICTS/qt2025/01).

* aritratkundu@gmail.com, aritra.kundu@uni.lu

- [1] S. Ramaswamy, Annual Review of Condensed Matter Physics **1**, 323 (2010), arXiv:1004.1933 [cond-mat].
- [2] K. Malakar, V. Jemseena, A. Kundu, K. V. Kumar, S. Sabhapandit, S. N. Majumdar, S. Redner, and A. Dhar, Journal of Statistical Mechanics: Theory and Experiment **2018**, 043215 (2018), arXiv:1711.08474 [cond-mat].
- [3] J. Tailleur and M. E. Cates, EPL (Europhysics Letters) **86**, 60002 (2009), arXiv:0903.3247 [cond-mat].
- [4] M. E. Cates and J. Tailleur, Annual Review of Condensed Matter Physics **6**, 219 (2015), arXiv:1406.3533 [cond-mat].
- [5] C. Maes, Journal of Physics A: Mathematical and Theoretical **50**, 381001 (2017).
- [6] B. D. Bruyne, S. N. Majumdar, and G. Schehr, Journal of Statistical Mechanics: Theory and Experiment **2021**, 043211 (2021), arXiv:2101.11895 [cond-mat].
- [7] H. M. Wiseman and G. J. Milburn, Physical Review A **47**, 642 (1993).
- [8] Z. K. Minev, Catching and Reversing a Quantum Jump Mid-Flight (2019), arXiv:1902.10355 [quant-ph].
- [9] K. W. Murch, S. J. Weber, C. Macklin, and I. Siddiqi, Nature **502**, 211 (2013).
- [10] S. Dhar, S. Dasgupta, and A. Dhar, Quantum time of arrival distribution in a simple lattice model (2015), arXiv:1312.5923 [quant-ph].
- [11] P. Singh, D. A. Kessler, and E. Barkai, Sokoban Random Walk: From Environment Reshaping to Trapping Transition (2025), arXiv:2508.07825 [cond-mat].
- [12] R. Yin, Q. Wang, S. Tornow, and E. Barkai, Proceedings of the National Academy of Sciences **122**, e2402912121 (2025).
- [13] R. Yin, Q. Wang, S. Tornow, and E. Barkai, The Journal of Chemical Physics **162** (2025), publisher: AIP Publishing.
- [14] J. G. Muga, J. P. Palao, and C. R. Leavens, Physics Letters A **253**, 21 (1999), arXiv:quant-ph/9803087.

[15] A. Tilloy, M. Bauer, and D. Bernard, *Physical Review A* **92**, 052111 (2015), arXiv:1510.01232 [quant-ph].

[16] C. Bernardin, R. Chetrite, R. Chhaibi, J. Najnudel, and C. Pellegrini, *The Annals of Applied Probability* **33**, 417 (2023).

[17] T. Benoist, C. Bernardin, R. Chetrite, R. Chhaibi, J. Najnudel, and C. Pellegrini, *Commun. Math. Phys.* **387**, 1821 (2021), eprint: 2103.01916.

[18] T. Benoist and C. Pellegrini, *Communications in Mathematical Physics* **331**, 703 (2014).

[19] J. M. Horowitz, *Physical Review E* **85**, 10.1103/physreve.85.031110 (2012).

[20] A. Sherry, C. Bernardin, A. Dhar, A. Kundu, and R. Chetrite, *Physical Review A* **111**, 042215 (2025), publisher: American Physical Society.

[21] P. A. M. Dirac, *Fundamental Interactions in Physics and Astrophysics: A Volume Dedicated to P.A.M. Dirac on the Occasion of his Seventieth Birthday*, , 354 (1973).

[22] A. P. Antonov, Y. Zheng, B. Liebchen, and H. Löwen, *Physical Review Research* **7**, 033008 (2025), arXiv:2305.16131 [cond-mat].

[23] To be published later: $p = \beta - \frac{\alpha^2}{3}$ and $q = \frac{2\alpha^3}{27} - \frac{\alpha\beta}{3} + \delta$ with $\alpha = -2\frac{v_d}{D}$, $\beta = \frac{1}{D^2}(v_d^2 - v^2 - 2D\lambda)$ and $\delta = \frac{2\lambda}{D^2}v_d$.

[24] F. Roccati, *Physical Review A* **104**, 022215 (2021), arXiv:2105.01197 [quant-ph].

[25] M. E. Cates, *Reports on Progress in Physics* **75**, 042601 (2012), arXiv:1208.3957 [cond-mat].

[26] To match the specific physical system introduced in [28] in the context of a stochastic non-hermitian Hamiltonian, we perform the parameter mapping: $\gamma_{\text{eff}} = \gamma\Gamma_e^2$ $\gamma' = -\Gamma_e + 2\gamma\Gamma_e^2$.

[27] See Appendix

[28] P. Martinez-Azcona, A. Kundu, A. Saxena, A. d. Campo, and A. Chenu, *Quantum Dynamics with Stochastic Non-Hermitian Hamiltonians* (2024), arXiv:2407.07746.

[29] P. Kumar, A. Romito, and K. Snizhko, *Physical Review Research* **2**, 043420 (2020), publisher: American Physical Society.

[30] V. Dubey, C. Bernardin, and A. Dhar, *Physical Review A* **103**, 032221 (2021).

[31] V. Dubey, R. Chetrite, and A. Dhar, *Journal of Physics. A. Mathematical and Theoretical* **56**, Paper No. 154001, 26 (2023).

[32] M. Naghiloo, M. Abbasi, Y. N. Joglekar, and K. W. Murch, *Nature Physics* **15**, 1232 (2019).

[33] A. Barchielli and M. Gregoratti, *Quantum trajectories and measurements in continuous time: the diffusive case*, Vol. 782 (Springer Science & Business Media, 2009).

[34] V. P. Belavkin, *Physics Letters. A* **140**, 355 (1989).

[35] P. Rouchon, A tutorial introduction to quantum stochastic master equations based on the qubit/photon system (2022), arXiv:2208.07416.

[36] R. Chetrite and H. Touchette, *Annales Henri Poincaré* **16**, 2005 (2015), arXiv:1405.5157 [cond-mat].

[37] G. Perfetto, F. Carollo, and I. Lesanovsky, *SciPost Physics* **13**, 079 (2022).

[38] J. Cornelius, Z. Xu, A. Saxena, A. Chenu, and A. d. Campo, *Physical Review Letters* **128**, 190402 (2022), arXiv:2108.06784 [quant-ph].

[39] Another approach is to first average over the noise, and only then impose trace preservation, which was studied in [28]. These two approaches will generally yield different dynamics.

[40] With $\langle \rho \rangle = \rho$.

[41] With $p = 4 - \frac{3\gamma_{\text{eff}}^2 - 3\gamma_{\text{eff}}\gamma' + \gamma'^2}{12}$, and $q = -\gamma_{\text{eff}} + \gamma'\frac{\gamma_{\text{eff}}^2 - \gamma_{\text{eff}}\gamma' + 8}{24} + \frac{\gamma'^3}{108}$.

[42] M. H. Devoret, J. M. Martinis, and J. Clarke, *Physical Review Letters* **55**, 1908 (1985).

[43] M. H. Devoret and R. J. Schoelkopf, *Science* **339**, 1169 (2013), publisher: American Association for the Advancement of Science.

[44] K. Zyczkowski and I. Bengtsson, *Geometry of quantum states* (2006).

[45] B. Misra and E. C. G. Sudarshan, *Journal of Mathematical Physics* **18**, 756 (1977).

[46] E. C. G. Sudarshan, *Pramana* **6**, 117 (1976).

[47] A. G. Kofman and G. Kurizki, *Nature* **405**, 546 (2000), publisher: Nature Publishing Group.

[48] A. Z. Chaudhry and J. Gong, *Zeno and anti-Zeno effects on Dephasing* (2014), arXiv:1402.5228 [quant-ph].

Characteristic function of p-RTP

We first study the persistent Run-and-Tumble particle (p-RTP) subject to a constant background drift v_d . This system maps to the Hamiltonian with $\hat{p} = i\partial_x$:

$$H_0 = i(v_d\mathbb{I} + v\sigma_z)\hat{p} + \lambda(\mathbb{I} - \sigma_x) - D\hat{p}^2\mathbb{I} \quad (9)$$

Defining the state vector as $|\mathbf{p}\rangle = \begin{pmatrix} p_+ \\ p_- \end{pmatrix}$, the corresponding Fokker-Planck equation is diagonal in their advective fluxes:

$$\partial_t |\mathbf{p}\rangle = H_0 |\mathbf{p}\rangle \quad (10)$$

We begin with the two steady-state ODEs and the boundary conditions. First, we sum the two ODEs: With $P(x) = P_+(x) + P_-(x)$ and $M(x) = P_+(x) - P_-(x)$, we have

$$D \frac{dP}{dx} - \mu P - vM = \text{const} \quad (11)$$

The total current is $J(x) = J_+(x) + J_-(x)$. Comparing this with Eq. (11), we see $\partial_x J = 0$. The boundary conditions stat

$$J(x) \equiv 0 \quad \forall x \in [-\ell, \ell] \quad (12)$$

This gives the crucial algebraic relation:

$$\mu P(x) + vM(x) - DP'(x) = 0 \quad (13)$$

which we solve for $M(x)$:

$$M(x) = \frac{D}{v}P'(x) - \frac{\mu}{v}P(x) \quad (14)$$

To get a single ODE for $P(x)$, we differentiate Eq. (14):

$$M'(x) = \frac{D}{v}P''(x) - \frac{\mu}{v}P'(x)M''(x) = \frac{D}{v}P'''(x) - \frac{\mu}{v}P''(x) \quad (15)$$

After some straightforward manipulation we get the following ODE, which gives the characteristic in main text

$$D^2 P'''(x) - 2D\mu P''(x) + (\mu^2 - v^2 - 2\lambda D)P'(x) + 2\lambda\mu P(x) = 0 \quad (16)$$

Standard RTP: ($D \rightarrow 0$)

For $D = 0$, the system reduces to: The stationary solution satisfies:

$$\frac{d}{dx}[(v_0 + v)p_+] = -\lambda p_+ + \lambda p_-, \quad \frac{d}{dx}[(v_0 - v)p_-] = \lambda p_+ - \lambda p_-.$$

Adding these equations gives zero total current and this integrates to:

$$p_+(x) = Ae^{r_1 x}, \quad \text{where } r_1 = \frac{2\gamma v_0}{v^2 - v_0^2}.$$

The total density is:

$$P(x) = p_+ + p_- = Ae^{r_1 x} \left(1 - \frac{v_0 + v}{v_0 - v} \right) = \frac{2v}{v - v_0} Ae^{r_1 x}.$$

Thus, the bulk solution is $P(x) = C_1 e^{r_1 x}$.

At the boundaries, particles accumulate due to reflection, forming delta functions. The boundary masses are determined by balance between incoming flux and tumbling:

$$(v_0 + v)p_+(\ell) = \gamma m_+, \quad (v_0 - v)p_-(-\ell) = \gamma m_-.$$

Using $p_+(\ell) = Ae^{r_1 \ell}$ and $p_-(-\ell) = -\frac{v_0 + v}{v_0 - v}Ae^{-r_1 \ell}$, we find:

$$m_+ = \frac{v_0 + v}{\gamma} Ae^{r_1 \ell}, \quad m_- = \frac{v_0 + v}{\gamma} Ae^{-r_1 \ell}.$$

Normalization requires:

$$\int_{-\ell}^{\ell} C_1 e^{r_1 x} dx + m_+ + m_- = 1.$$

Solving for C_1 and A , we obtain:

$$C_1 = \frac{r_1}{2} \left[\sinh(r_1 \ell) + \frac{v_0}{v} \cosh(r_1 \ell) \right]^{-1}, \quad A = \frac{v - v_0}{2v} C_1.$$

The masses become:

$$m_{\pm} = \frac{1}{2} \frac{v_0}{v} \frac{e^{\pm r_1 \ell}}{\sinh(r_1 \ell) + \frac{v_0}{v} \cosh(r_1 \ell)}$$

Thus, the full solution is:

$$P_C(x) = \frac{r_1}{2} \frac{e^{r_1 x}}{\sinh(r_1 \ell) + \frac{v_0}{v} \cosh(r_1 \ell)} + m_{\pm} \delta(x \pm \ell)$$

$D \rightarrow \infty$ Limit

As $D \rightarrow \infty$, the system reduces to drift-diffusion with drift v_0 :

$$\frac{P'(x)}{P(x)} \approx \frac{v_0}{D}.$$

The solution is:

$$P_C(x) \approx \frac{v_0/(2D)}{\sinh(v_0 \ell / D)} \exp\left(\frac{v_0}{D} x\right).$$

Expanding for small $v_0 \ell / D$:

$$P_C(x) \approx \frac{1}{2\ell} \left(1 + \frac{v_0}{D} x \right).$$

EXPRESSIONS FOR BIASED QUANTUM TRAJECTORY

In small diffusion Limit ($D \rightarrow 0$), the distribution is defined on the domain $X \in [-\epsilon, \epsilon]$.

$$P(X) = \mathcal{A} \frac{(1 + X)^{\frac{r_1}{2} - 1}}{(1 - X)^{\frac{r_1}{2} + 1}} + m_{\delta}^{\pm} \delta(X - \pm\epsilon)$$

where,

$$r_1 = \frac{4\lambda J}{\gamma'^2 - 4J^2}$$

$$\mathcal{A} = \frac{r_1/2}{\sinh(r_1 \ell) + \frac{v_0}{v} \cosh(r_1 \ell)}$$

$$m_{\delta}^{\pm} = \frac{1}{2} \frac{v_0}{v} \frac{e^{\pm r_1 \ell}}{\sinh(r_1 \ell) + \frac{v_0}{v} \cosh(r_1 \ell)}$$

In large diffusion Limit ($D \rightarrow \infty$), the asymptotic distribution for large diffusion (small Péclet number) is:

$$P(X) \approx \frac{1}{2\ell} \left[1 - \frac{\gamma'}{\gamma_{\text{eff}}} \text{arctanh}(X) \right] \frac{1}{1 - X^2}$$

TILTED BELAVKIN–BARCHIELLI DYNAMICS

The unnormalized conditional state $\check{\varrho}_t$ obeys the linear Zakai equation

$$d\check{\varrho}_t = \mathcal{L}_{\text{eff}}[\check{\varrho}_t] dt + \sqrt{2\gamma} \mathcal{M}[\hat{L}] \check{\varrho}_t dY_t, \quad (17)$$

where

$$\mathcal{L}_{\text{eff}}[\varrho] = -i[\hat{H}, \varrho] + \gamma(2\hat{L}\varrho\hat{L}^{\dagger} - \{\hat{L}^{\dagger}\hat{L}, \varrho\}), \quad (18)$$

$$\mathcal{M}[\hat{L}]\varrho = \hat{L}\varrho + \varrho\hat{L}^\dagger, \quad (19)$$

and Y_t is a Wiener process.

To bias the measurement record, we introduce the exponential martingale $M_t^{(s)} = \exp(sY_t - \frac{1}{2}s^2t)$ and define the tilted measure $d\mathbb{P}^{(s)} = M_t^{(s)}d\mathbb{P}$. The tilted unnormalized state $\tilde{\varrho}_t = M_t^{(s)}\varrho_t$ then satisfies

$$d\tilde{\varrho}_t = \left(\mathcal{L}_{\text{eff}} + s\sqrt{2\gamma} \mathcal{M}[\hat{L}] \right) \tilde{\varrho}_t dt + \left(\sqrt{2\gamma} \mathcal{M}[\hat{L}] + s \right) \tilde{\varrho}_t dY_t. \quad (20)$$

Writing $\hat{\varrho}_t = \tilde{\varrho}_t/\text{Tr}(\tilde{\varrho}_t)$ one obtain by Girsanov's theo-

rem, under $\mathbb{P}^{(s)}$ the innovation process

$$d\tilde{W}_t = dY_t - (\sqrt{2\gamma}\langle \hat{X}_L \rangle_t + s)dt \quad (21)$$

is a standard Wiener process. The normalized dynamics therefore takes the compact form

$$d\hat{\varrho}_t = \mathcal{L}_{\text{eff}}[\hat{\varrho}_t] dt + \sqrt{2\gamma} \mathcal{H}[\hat{L}] \hat{\varrho}_t (d\tilde{W}_t + s dt) \quad (22)$$

with the associated signal equation

$$dY_t = (\sqrt{2\gamma}\langle \hat{X}_L \rangle_t + s)dt + d\tilde{W}_t. \quad (23)$$